Multiferroic phase diagram of *E*-type $R\mathrm{MnO_3}$ films studied by neutron and x-ray diffraction

Saumya Mukherjee,[1,2,*] Kenta Shimamoto,[3] Yoav William Windsor,[4] Mahesh Ramakrishnan,[4] Sergii Parchenko,[4] Urs Staub,[4] Laurent Chapon,[1,5] Bachir Ouladdiaf,[5] Marisa Medarde,[6] Tian Shang,[6,4] Elisabeth A. Müller,[7] Michel Kenzelmann,[2,6] Thomas Lippert,[8,3] Christof W. Schneider,[3] and Christof Niedermayer[2,†]

[1]*Diamond Light Source, Oxfordshire OX11 0DE, United Kingdom*
[2]*Laboratory for Neutron Scattering and Imaging, Paul Scherrer Institut, 5232 Villigen PSI, Switzerland*
[3]*Laboratory for Multiscale Materials Experiments, Paul Scherrer Institut, CH 5232 Villigen-PSI, Switzerland*
[4]*Swiss Light Source, Paul Scherrer Institut, CH 5232 Villigen-PSI, Switzerland*
[5]*Institut Laue-Langevin, 71 Avenue des Martyrs, CS 20156, F-38042 Grenoble Cedex 9, France*
[6]*Laboratory for Scientific Development and Novel Materials, Paul Scherrer Institut, CH 5232 Villigen-PSI, Switzerland*
[7]*Electron Microscopy Facility, Paul Scherrer Institut, CH 5232 Villigen-PSI, Switzerland*
[8]*Laboratory of Inorganic Chemistry, Department of Chemistry and Applied Biosciences, ETH Zürich, CH 8093 Zurich, Switzerland*

(Received 12 June 2017; revised manuscript received 23 August 2018; published 13 November 2018)

We present a generalized multiferroic phase diagram for orthorhombic $R\mathrm{MnO_3}$ (R = Gd–Lu) based on coherently grown thin films. The magnetic order was identified by neutron-diffraction and resonant soft x-ray scattering experiments. For large R-ions (R = Gd–Dy), the transition temperature to a long-range ordered antiferromagnetic phase is only weakly dependent on the R-ion radius, but decreases monotonically with decreasing R-ion radius for films with R = Ho–Lu. The antiferromagnetic phase is characterized by an incommensurate order of the Mn^{3+} spins, which successively locks into a commensurate E-type state. These findings confirm a uniform multiferroic ground state independent of the R ion and are in excellent agreement with predicted properties of strain-induced multiferroicity in these materials. In particular, strong variation of multiferroic properties in these epitaxial films compared to bulk highlights the tuning ability of strain.

DOI: 10.1103/PhysRevB.98.174416

I. INTRODUCTION

The unique coexistence of magnetic and electric order parameters together with the ability to cross couple their response to external fields makes magnetoelectric multiferroics interesting both from a fundamental perspective and in terms of future applications [1]. Multiferroicity in rare-earth manganites ($R\mathrm{MnO_3}$), which crystallize in an orthorhombic (o-) phase with a *Pbnm* crystal symmetry, has been widely studied to understand the microscopic role of the competing interactions [2,3]. Depending on the R-ion radius, o-$R\mathrm{MnO_3}$ feature a variety of multiferroic ground states. $\mathrm{TbMnO_3}$ with a larger R-ion radius possesses a ferroelectric (FE) polarization along the c axis, which is induced by an incommensurate (ICM) cycloidal antiferromagnetic (AFM) order that originates from an antisymmetric magnetostriction mechanism [2,4,5]. In contrast, the FE order along the a axis in $\mathrm{YMnO_3}$ with a smaller R-ion radius is induced by a commensurate (CM) E-type magnetic order associated with a symmetric magnetostriction [3,6,7].

The magnetic and electric order parameters in o-$R\mathrm{MnO_3}$ can be tuned by both physical and chemical pressure and this results in ground states with improved multiferroic properties [8–11]. The growth of epitaxial thin films on crystalline substrates is an alternative way to control multiferroicity [12–14], since the lattice mismatch between the substrate and the sample induces strain and a structural reconfiguration. This leads to remarkable changes of the physical properties. Notable examples include strain-induced ferroelectricity in $\mathrm{SrTiO_3}$ at room temperature and the appearance of FE and ferromagnetic (FM) order in $\mathrm{EuTiO_3}$ when grown under epitaxial strain [15,16].

One of the earlier attempts to grow o-$R\mathrm{MnO_3}$ thin films under strain were made on $\mathrm{TbMnO_3}$ and $\mathrm{YMnO_3}$, showing different multiferroic ground states [17–19]. Control over multiferroicity using strain was also highlighted in $\mathrm{HoMnO_3}$ [20] and $\mathrm{TmMnO_3}$ [21] along with $\mathrm{LuMnO_3}$ [22] and $\mathrm{YMnO_3}$ [23]. The most dramatic effect was observed in an anisotropically strained epitaxially grown (010)-oriented $\mathrm{TbMnO_3}$ thin film [24]. A modified multiferroic ground state characterized by an E-type AFM phase was observed together with a switching of the orientation of the FE polarization (P) along the a axis. In addition a significant increase in the magnitude of P was found with respect to bulk. This confirmed that the dominant role of the antisymmetric mechanism for multiferroicity in bulk $\mathrm{TbMnO_3}$ was replaced by the symmetric spin exchange interaction on the application of epitaxial strain.

These modifications of the FE properties of $\mathrm{TbMnO_3}$ were shown to exist for the entire series of o-$R\mathrm{MnO_3}$ (R = Gd–Lu) thin films [25]. In each case, a transition from a paramagnetic (PM) to an AFM phase followed by a transition to a FE phase was observed. The AFM transition temperature was identified by magnetic susceptibility measurements, defined here as T_M, and the FE transition temperature T_FE by dielectric

*saumya.mukherjee@psi.ch
†christof.niedermayer@psi.ch

measurements. These studies revealed that the magnetically induced FE phase remains largely independent of the R ion. We therefore proposed a common multiferroic ground state in strain stabilized o-RMnO$_3$ films. However, except for TbMnO$_3$, no direct evidence on the magnetic order of these films was presented and the role of R ion remained unclear.

In the present paper, we intend to gain a better understanding of the magnetic order of (010)-oriented epitaxial o-RMnO$_3$ (R = Gd–Lu) thin films coherently grown on (010) YAlO$_3$ substrates. Our data strongly support the multiferroic ground state proposed in reference [25]. We will also present and discuss a multiferroic phase diagram of these strained films in terms of the observed ordering temperatures and illustrate the role of the R ion. To study the magnetic order we combined the complementary capabilities of neutron scattering and resonant soft x-ray diffraction (RSXD). We identify a R-ion radius dependent variation of the transition temperature to an ICM AFM state (T_N). The ICM phase was found to lock into a robust commensurate E-type order at $T_{\text{lock-in}}$. Our results are in agreement with the proposed change of the multiferroic mechanism due to strain [24,25] which was shown to stabilize the E-type order and induce a large FE polarization along the a axis. The onset of the FE order occurs in the ICM phase independent of the E-type ordering, unlike in bulk o-RMnO$_3$ (R = Ho–Lu) [26–29]. We also address the role of the $4f$ rare-earth and $3d$ Mn magnetic order interplay. In this paper, we therefore present a comprehensive and generalized overview of the R-ion-radius-dependent multiferroic phase diagram of epitaxially strained o-RMnO$_3$ thin films.

II. SAMPLES AND CHARACTERIZATION

Epitaxial o-RMnO$_3$ films were deposited on (010)-oriented o-YAlO$_3$ substrates using pulsed laser deposition as discussed elsewhere [25]. The thickness of the films varied between ($t \sim$ 10–44 nm). The crystallinity and the change in lattice parameters due to strain were determined by x-ray diffraction.

To investigate the magnetic ground state of the RMnO$_3$ films, we performed neutron-diffraction experiments on the cold-neutron triple-axis spectrometer RITA-II at the Swiss Spallation Neutron Source (SINQ), PSI, and the thermal-neutron single crystal four-circle diffractometer D10 at the Institut Laue-Langevin (ILL). The incident wavelengths of $\lambda_{\text{RITA-II}} = 4.21$Å and $\lambda_{\text{D10}} = 2.364$ Å were obtained from the (0 0 2) Bragg reflection of pyroelectric graphite (PG) monochromators. At RITA-II, a collimation of 80' and a PG filter were placed between the monochromator and the sample and a cooled Be filter was introduced between the sample and the analyzer to prevent higher order contaminations. A nine-blade analyzer [30] and a coarse adjustable collimator before a position-sensitive ^{3}He detector provides high q-resolution and guarantees an excellent signal-to-noise ratio. This setup enables us to measure the elastic magnetic signal from the thin films despite the very small sample volume. All samples were mounted in a He-flow cryostat with the (00l)-(0k0) crystal axis in the scattering plane to give access to the strong magnetic reflections for an E-type structure. At D10, a circular aperture of 12 mm was inserted between the monochromator and the sample. We used a vertical-focusing PG analyzer between the sample and the single ^{3}He detector.

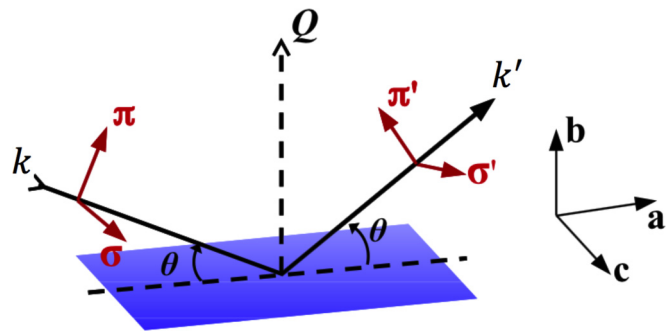

FIG. 1. Experimental geometry for RSXD using linearly polarized incident and scattered light. The scattering wave vector $\mathbf{Q} = (k' - k)$ is along the b axis, where k (k') is the incoming (outgoing) wave vector of light.

A collimation of 20' was placed before the detector. The four-circle setup at D10 allowed accessing reflections in the (hkl) scattering planes.

Resonant soft x-ray diffraction (RSXD) at the RESOXS UHV diffraction end station [21,22,31] at the SIM beam line [32] of the Swiss Light Source (SLS), Paul Scherrer Institut (PSI) was used in addition to study the magnetic order of GdMnO$_3$. RSXD allows us to probe the $3d$ magnetic states of Mn ions due to electric-dipole transition from $2p$ to the $3d$ states at the absorption edges. The experimental scattering geometry for the sample is shown in Fig. 1 and similar to the setup used in Ref. [21]. Measurements were done with a photon energy tuned to the Mn $L_{2,3}$ absorption edges using linearly polarized incident light [horizontal (π) and vertical (σ)] with respect to the scattering plane. The scattering intensity of the polarized light is collected using an IRD AXUV100 photo diode. All samples were mounted on a cold head of a Janis flow cryostat with a base temperature of 10 K.

For the study of the in-plane electric properties in an applied magnetic field, temperature-dependent capacitance measurements were performed on a physical properties measurement systems (PPMS-9T, Quantum Design) with a homemade sample holder. To apply the external electric field, interdigitated electrodes were sputtered onto the films as discussed in Refs. [20,24,25]. The capacitance was measured using an Agilent E4980 LCR meter with zero DC bias voltage and an AC voltage of 100 mV between 13 kHz and 1.3 MHz. Here, we only present the data taken at 13.3 kHz [24].

III. RESULTS AND DISCUSSION

A. Structural properties

Orthorhombic (010)-oriented RMnO$_3$ films ($Pbnm$ space group) were grown by PLD. The a and c parameters of the films are locked to the YAlO$_3$ substrate in-plane lattice parameters [$a \approx 5.185(\pm 0.005)$ Å, $c \approx 7.37(\pm 0.01)$ Å] [25], while the b axis lattice parameter depends on the R-ion size and varies between $+1.9\%$ for R = Gd and -0.26% for R = Lu as a consequence of the induced strain (see Table I). As reported in Ref. [25], all films show a compressive strain along the a axis while the strain along the c axis varies with the radius of the R ions. The films are compressively strained along c for R = Gd–Dy, and have a tensile strain for

TABLE I. Multiferroic transition temperatures of o-RMnO$_3$[a].

RMnO$_3$	η_b %	t_R (nm)	T_N (K) bulk	T_N (K) Film	T_{FE} (K) Bulk	T_{FE} (K) Film	$T_{lock\text{-}in}$ (K) Bulk	$T_{lock\text{-}in}$ (K) Film	T_N^R (K) Bulk	T_N^R (K) Film
GdMnO$_3$	+1.9	10	43	41	8(15)	39	23	–	6.5	10
TbMnO$_3$	+1.7	44	41	41	28	41	28	31	7	8
DyMnO$_3$	+1.2	16	39	42	18	36	18	30	6.5	8
HoMnO$_3$	+0.7	17.5	41	41	26	39	26	30	6.5	8
ErMnO$_3$	+0.85	38	42	39	28	37	28	31	–	–
TmMnO$_3$	−0.02	16	42	38	32	35	32	28	4	–
YbMnO$_3$	−0.26	17	43	37	37	34	36	–	4	8
LuMnO$_3$	−0.26	13	39	36	36	32	35.5	31	–	–

[a]References: bulk parameters of GdMnO$_3$ [34,56,57], TbMnO$_3$ [4,34], DyMnO$_3$ [34,58], HoMnO$_3$ [26,34], ErMnO$_3$ [29], TmMno$_3$ [39], YbMnO$_3$ [28,38], LuMnO$_3$ [27], and T_{FE} of RMnO$_3$ films [24,25], and T_N of TbMnO$_3$ film[24].

R = Ho–Lu. As a result of the interplay between tensile and compressive strain along the different crystalline directions and the elastic properties of the material, the volume of the unit cell is not preserved. With the b axis expanded and the a and c lattice parameter locked to the lattice of the substrate, the film-unit cell volume is smaller than the volume for the bulk-unit cell. To illustrate the coherent growth of these films, electron diffraction images for a 100-nm (010) HoMnO$_3$ are shown in Fig. 2 with (a) the cut along the (001) and (b) the (100) in-plane direction. The extracted in-plane lattice parameters are $a \approx 5.18$ Å and $c \approx 7.35$ Å for the substrate and $a \approx 5.26$ Å and $c \approx 7.37$ Å for the 100 nm HoMnO$_3$ film. These numbers show, even for such a thick film, much thicker than the magnetic and electric properties of RMnO$_3$ films presented, the crystalline coherence with respect to the c direction is still maintained [see Fig. 2(a)] whereas the coherence along the a direction is not fully preserved [see Fig. 2(b)] and consistent with XRD measurement shown in Ref. [20]. It is therefore expected that the unique alteration of the unit cell is crucial in defining the interatomic interactions and as a consequence the modification of the magnetic and FE orders.

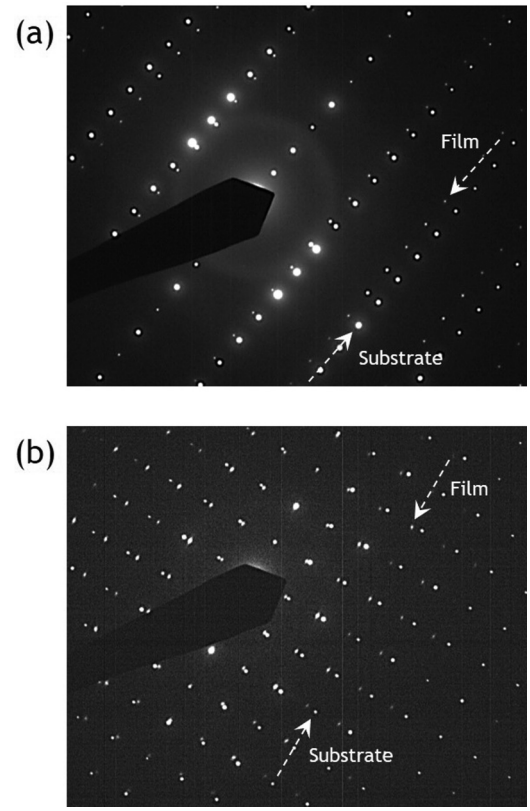

FIG. 2. Electron diffraction image of a 100 nm (010)-oriented o-HoMnO$_3$ film grown on (010) YAlO$_3$. (a) Diffraction image of a section cut along the (001) in-plane direction. The rows of diffraction spots for the film and substrate are marked with arrows. (b) Diffraction image of a section cut along the (100) in-plane direction. The rows of diffraction spots for the film and substrate are marked with arrows.

B. Magnetic properties

Recently we reported spontaneous FE ordering [25] along the a axis with $T_{FE} \sim 39$ K and an appreciably large polarization $P_a \sim 1\,\mu$C/cm^2 for a series of strained o-RMnO$_3$ (R = Gd–Lu) films. These strain-modified electrical properties implied the stabilization of an E-type magnetic order not found in bulk for most of the o-RMnO$_3$ compounds. The magnetic order of these highly strained films is probed using neutron and RSXD. A detailed description of the magnetic order is presented to explain the observed multiferroicity of these films [25].

1. Neutron diffraction studies

Neutron diffraction gives access to a large Ewald sphere and enables us to measure the intensity of $\mathbf{Q} = (0\,q\,1)$ reflection for the family of strained o-RMnO$_3$ (R = Gd–Lu) thin films. Magnetic structure factor calculations indicate that the $(0\,q\,1)$ reflection is one of the strongest magnetic reflections of the observed ground state in o-RMnO$_3$, such as a spiral or an E-type phase [4,27]. The measured intensity of the magnetic reflections is sensitive to the projection of the magnetization components normal to $\mathbf{Q}$. This implies that by measuring $(0\,q\,1)$, we probe the magnetization components along the a, b, and c axis.

The temperature dependencies of the $(0\,q\,1)$ peak intensities and magnetic modulation wave vector (q) for strained o-RMnO$_3$ films are presented in Fig. 3. For GdMnO$_3$, the magnetic order of the Mn spins is very close to an E-type order below $T = 10$ K with $q \approx 1/2$. The onset of the peak intensity yields $T_N \sim 41$ K consistent with previous results [25]. The peak intensity of $(0\,q\,1)$ at $q \approx 1/2$ features a sharp increase of $\Delta I \sim 110\%$ due to the ordering of the Gd moments below $T_N^{Gd} \sim 10$ K. The fact that the Gd and the Mn order are described by the same propagation wave vector is evidence for an effective magnetization and an interplay of the unpaired $4f$ electrons of the Gd ions with $3d$ electrons of the Mn ions in the GdMnO$_3$ film below T_N^{Gd}. Compared to bulk ($T_{N,bulk}^{Gd} \sim 6.5$ K) [33], the strained GdMnO$_3$ thin film shows an increase in the Gd ion ordering temperature.

Magnetic order with a similar q was also observed for other o-RMnO$_3$ (R = Tb - Yb) films with smaller R-ion radii ($r_R < r_{Gd}$) [see Figs. 3(b)–3(f) (inset)]. These films exhibit a tensile strain (η_b%) along the b axis (see Table I) and the magnetic transition to the ICM AFM phase occurs at

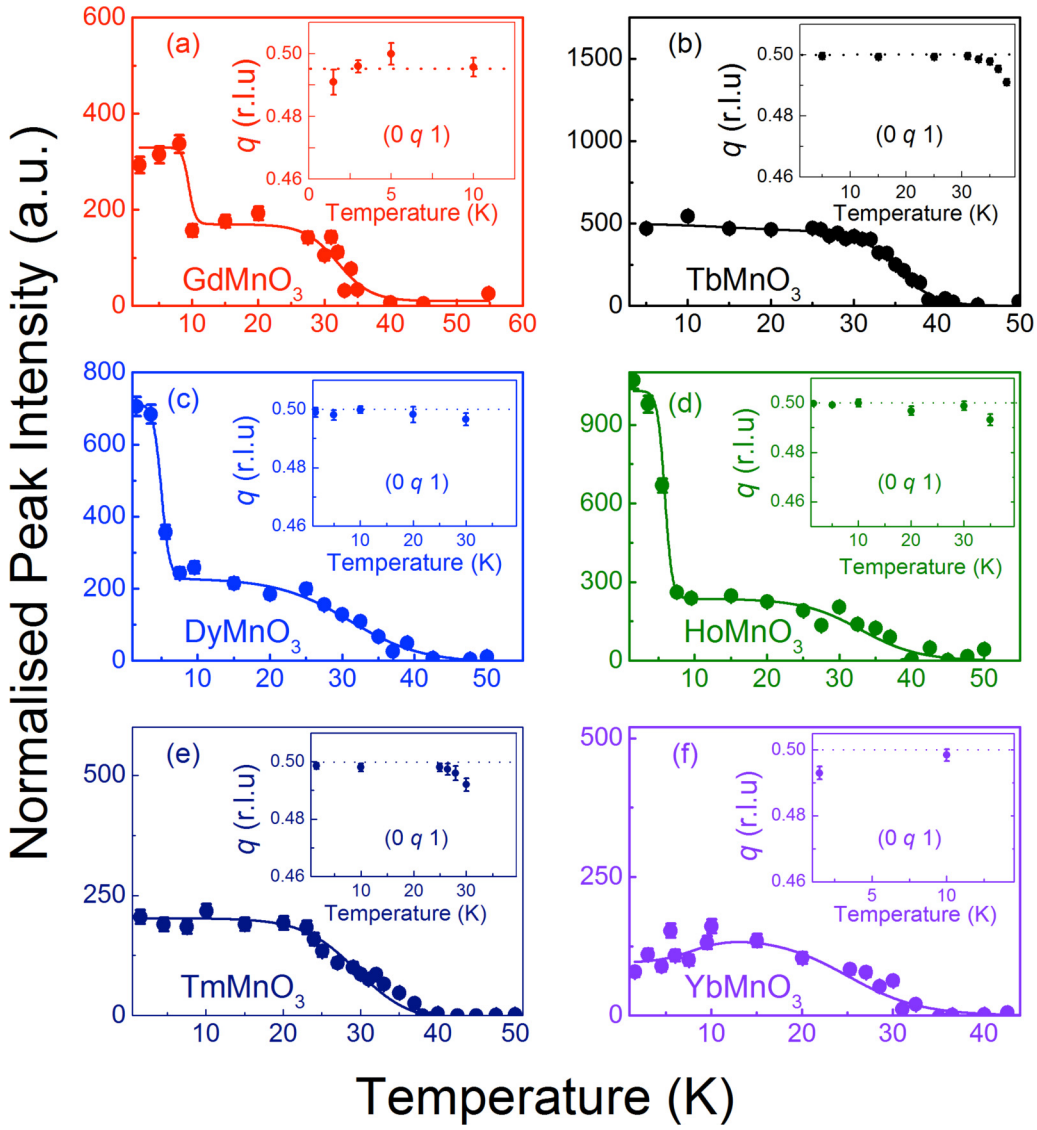

FIG. 3. Normalized peak intensity of $(0\,q\,1)$ reflection and magnetic modulation wave vector (inset) of (a) $GdMnO_3$, (b) $TbMnO_3$, (c) $DyMnO_3$, (d) $HoMnO_3$, (e) $TmMnO_3$, and (f) $YbMnO_3$. The solid lines are guide to eye and dotted lines (inset) mark the commensurate order at $q_{Mn} = 0.5\mathbf{b}^*$.

$T_N \approx 37$–41 K with $q < 1/2$ [Figs. 3(b)–3(f)]. The ICM phase is found to undergo a FE transition at $T_{FE} \approx 34$–41 K with a spontaneous polarization along the a axis, replicating the electric properties of $GdMnO_3$ films [24,25]. The magnitude of the polarization (1–$2\,\mu C/cm^2$) is also comparable, which confirms the existence of a multiferroic ICM phase in these films. A second magnetic transition to a locked-in commensurate E-type phase with $q \sim 1/2$ occurs at a lock in temperature $T_{\text{lock-in}}$ for all the $RMnO_3$ films (R = Tb–Lu). For R = Gd, the film experiences the largest tensile strain along the b axis ($\eta_b \sim +1.9\%$) [25] ($\eta_b = [(b_{\text{film}} - b_{\text{bulk}})/b_{\text{bulk}}]$) and is possibly at the limit to exert tensile strain, which favors the stabilization of an E-type order. Contrary to bulk, no additional FE transition accompanies the onset of the E-type order below $T_{\text{lock-in}}$ [25].

The sharp increase (ΔI) in peak intensity of $(0\,q\,1)$ at T_N^R representing the rare earth ordering is found for o-$RMnO_3$ films as shown in Figs. 3(b)–3(c), except for $TbMnO_3$ and $TmMnO_3$. The most dramatic increase in peak intensity was observed for the ordering of R = Dy (∼350%) and Ho (∼450%) ions. For R = Yb, there is a lowering of the peak intensity below 8 K, indicating a change of the commensurate magnetic order of Mn spins. Evidence on Tb ordering was obtained by measuring the (0 1/2 2) reflection below T = 10 K. This reflection is sensitive to Tb ordering only [4] and the temperature dependence as shown in Fig. 4 confirms the ordering of the Tb spins below $T_N^{Tb} \sim 8$ K. Consistent with the magnetic order of other magnetic R ions, Tb spins stay locked to the commensurate phase with $q_{Tb} = 0.5\mathbf{b}^*$. However, the Tb ordering failed to induce an increase in the $(0\,q\,1)$ intensity, a magnetic Bragg peak which is sensitive to Mn and Tb ordering. Looking at the structure factors, both magnetic Bragg peaks should show up with a comparable intensity, which is not the case. This suggest a weak interaction of Tb and Mn spins. In addition, a representative rocking (omega) scan of the (0 1/2 2) reflection at $T = 4$ K with a FWHM

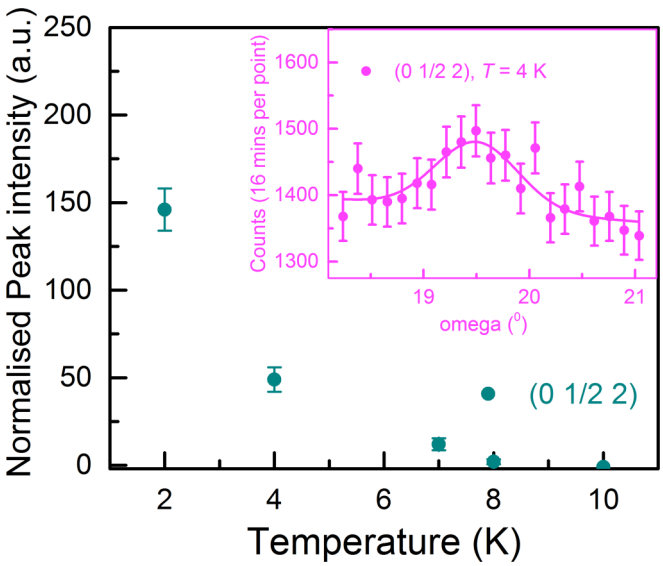

FIG. 4. Temperature-dependent appearance of the (0 1/2 2) reflection from the normalized peak intensity of $TbMnO_3$. Inset: (0 1/2 2) reflections measured at $T \sim 4$ K .

($\Delta\omega$) of 0.81° is shown as an inset to Fig. 4. The width of this peak is approximately three times wider than the equivalent omega scan for the (0 1/2 1) with $\Delta\omega = 0.24°$ corresponding to the experimental resolution of the instrument. Combined with the small intensity for the (0 1/2 2), this suggests that the Tb spins are short-range ordered. A microscopic understanding of this behavior is at present not available. Note, the ordering of R spins does not induce any anomaly in the dielectric susceptibility, unlike in bulk [34], and no change in the FE polarization is observed.

To discuss the peak intensity and magnetic order derived from (0 q 1) reflections, we show a set of representative q scans as a function of temperature (see Fig. 5) for R = Tb–Ho and Yb. The main feature is the (0 q 1) peak centered around $q \sim 0.5$. It also has the largest intensity except for R = Yb. The lowering of the peak intensity at $q \sim 1/2$ for $YbMnO_3$ is due to a change in the magnetic order of the Mn spins. A transition from the commensurate to an ICM phase occurs as indicated by the shift in the peak position to $q < 1/2$ at $T \sim 1.5$ K [see Fig. 5(d)]. This suggests that the E-type Mn order is suppressed owing to the Yb–Mn interaction. For $TbMnO_3$, the change in the magnetic order of Mn spins from an ICM phase at $T = 36.5$ K to an E-type phase below 31 K is represented by the peak shift toward $q \sim 1/2$ [24]. For R = Dy and Ho, the effect of the rare earth on the peak intensity of (0 q 1) is evident from the intensity growth at low temperatures.

Similar studies were also conducted on strained o-$LuMnO_3$ thin film with Lu being the element with the smallest R-ion

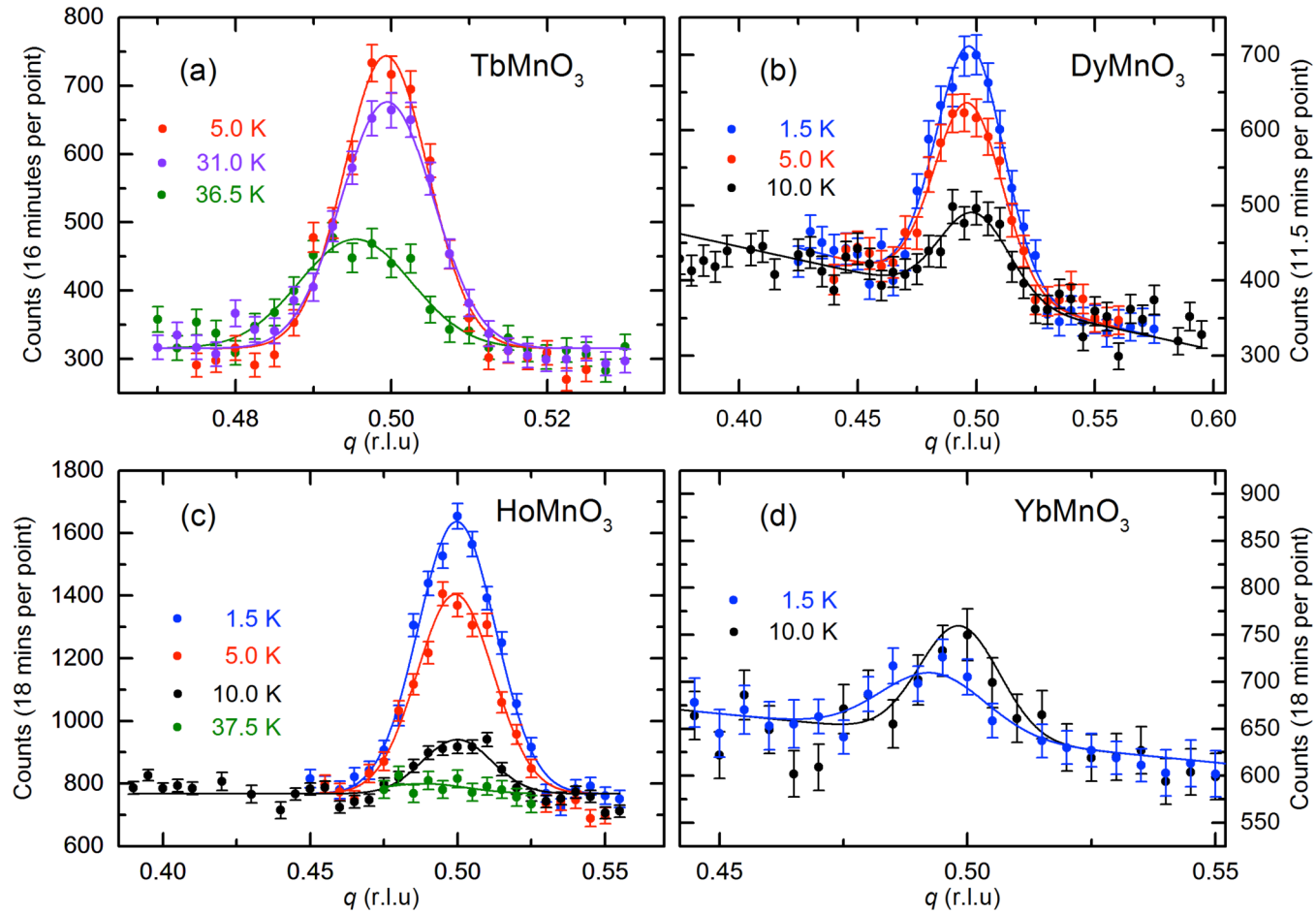

FIG. 5. Plots showing q scans for (0 q 1) magnetic reflections at different temperatures of (a) $TbMnO_3$, (b) $DyMnO_3$, (c) $HoMnO_3$, and (d) $YbMnO_3$.

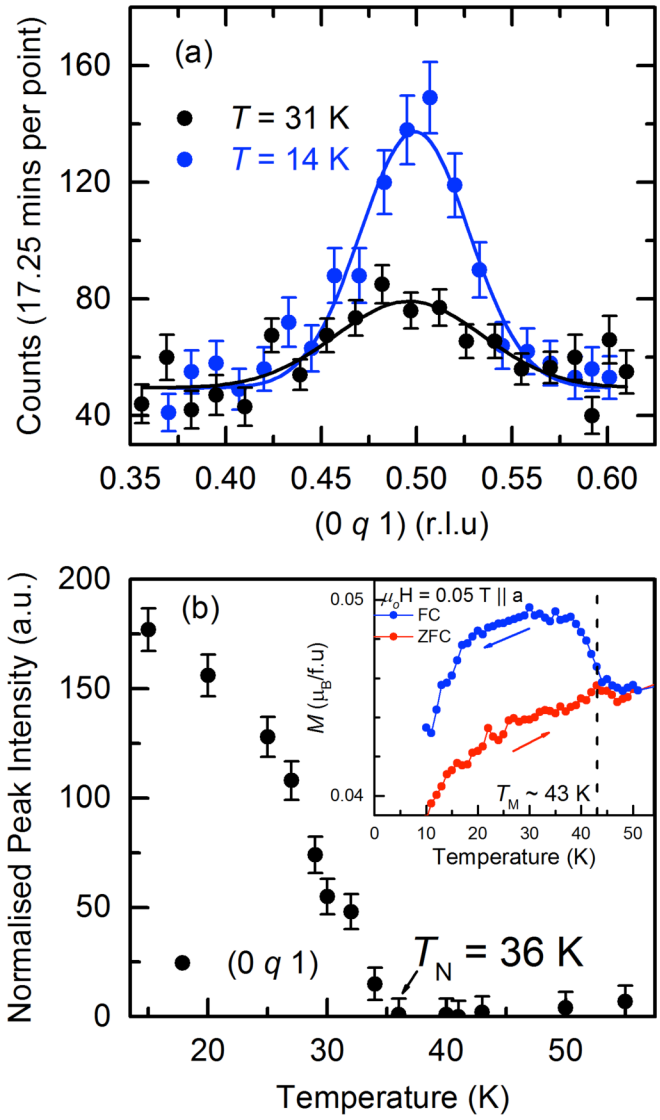

FIG. 6. (a) Magnetic reflections $(0\,q\,1)$ of $LuMnO_3$ measured at T =14 K and 31 K, (b) temperature dependence of $(0\,q\,1)$ peak intensity showing the T_N and (inset) magnetic susceptibility measurements showing T_M from Ref. [25].

radius. $LuMnO_3$ is unique since Lu^{3+} is nonmagnetic and therefore acts as an ideal prototype to study multiferroicity purely due to Mn spin ordering. Compared to other $RMnO_3$ (R = Gd–Yb) films, the magnetic ground state of strained $LuMnO_3$ film shows no change in q and represents an E-type order with $q = 1/2$ below $T_{\text{lock-in}} \sim 31$ K [see Fig. 6(a)]. However, the transition from a paramagnetic to an ICM phase occurs at a significantly lower $T_N \sim 36$ K, as marked in the temperature dependence of the $(0\,q\,1)$ peak intensity [see Fig. 6(b)]. We want to note that T_N is also lower than the magnetic ordering temperature T_M, derived from magnetic susceptibility measurements [Fig. 6(b) inset]. In addition, the $LuMnO_3$ film does not host FE within the ICM magnetic phase. The onset of FE polar ordering at $T_{FE} \sim 32$ K [25] and the E-type commensurate order at $T_{\text{lock-in}} \sim 31$ K occurs almost concurrently. This result shows that strained $LuMnO_3$ thin films qualitatively replicate bulk multiferroicity [27]. Considering that Lu has the smallest R radius and hence induces the largest distortions within the bulk $RMnO_3$ unit cell, it is not unreasonable to reach at some point in the generalized phase diagram more bulklike properties. The implications would be that the bulk lattice distortions for $LuMnO_3$ already modified the multiferroic interaction parameter to the maximum or at least close to the threshold value, which favors an E-type ground state. More strain induced via thin-film growth seems not necessarily beneficial in the context of improving multiferroic properties further. The other end of this strain scale would be the coherently strained $GdMnO_3$. The change in its unit cell volume is the largest among all the prepared $RMnO_3$ thin films. It experiences the largest compressive strain for the (100) and (001) in-plane orientation of the series of films grown on (010) $YAlO_3$ [25]. If an even larger compressive strain can be applied to convert o-$EuMnO_3$ or o-$SmMnO_3$ from an A-type AFM into an E-type is at present unknown.

2. *Resonant x-ray diffraction studies*

In this section, we present complementary measurements of the magnetic order of strained o-$GdMnO_3$ using RXSD and compare them with the results obtained from neutron diffraction. We collect diffraction signals using photon energies corresponding to the Mn $L_{2,3}$ absorption edges to probe the magnetic order of the Mn^{3+} ions.

We measured the magnetic reflection $(0\,q\,0)$, reachable in reciprocal space with the described experimental geometry and energy of the incident photon. In Fig. 7(a), the q-scan along the b^* axis of $(0\,q\,0)$ reflection measured at different temperatures is presented. It shows that the peak position shifts toward $q \approx 1/2$ and the intensity of the reflection increases with decreasing temperature. Additional weaker peaks at $q \approx 0.4$ with a similar temperature dependence represent AFM Kiessig fringes, which arise from the limited thickness of the magnetic layer. Similar features were also observed in antiferromagnetically ordered o-$YMnO_3$ thin films [23]. In addition, the peak at $q \approx 0.55$ and its corresponding intensity is independent of temperature, implying a nonmagnetic origin. The AFM transition temperature in $GdMnO_3$ was found at $T_N = 41$ K from the temperature dependence of the integrated intensity of $(0\,q\,0)$ [see Fig. 7(b)]. The variation of the magnetic periodicity with temperature represented by $q(T)$ confirmed that the ground state with $q < 0.5$ fails to lock in to a E-type order [inset, Fig. 7(b)]. These results coincide with the neutron-diffraction studies.

For E-type AFM order of the Mn spins in o-$RMnO_3$ with a $Pbnm$ symmetry and a collinear alignment of the moments along the b axis, the magnetic structure factor for the $\mathbf{Q} = (0\,1/2\,0)$ reflection is zero, which is not consistent with the experimentally observed scattering intensity at this q value. A finite structure factor can, however, arise from a nonzero staggered magnetization component along the c axis. A detailed analysis of the magnetization components can be done by performing an azimuthal scan. In this approach, the sample is rotated around $\mathbf{Q}$ and the scattered intensity is measured with polarized light.

A calculated intensity contribution of the magnetization components reproduces the observed variation of the scattered

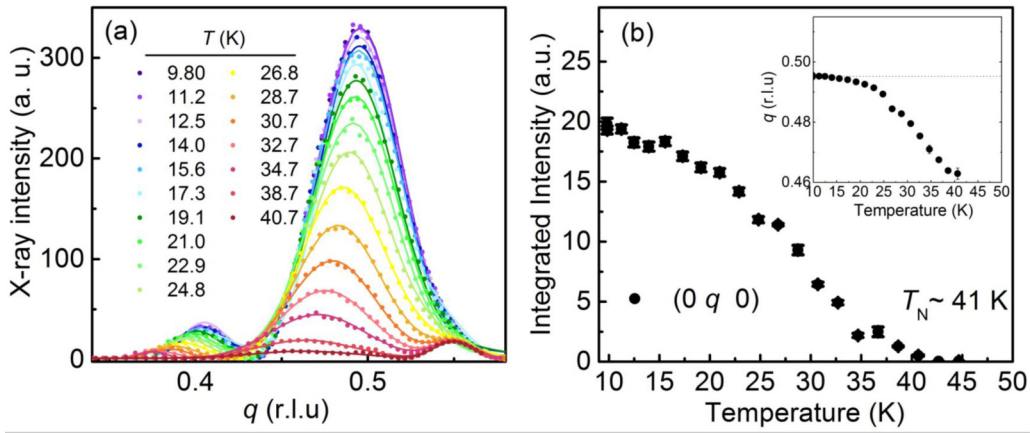

FIG. 7. (a) Temperature dependence of the magnetic reflection (0 q 0) of 10 nm (010)-oriented GdMnO$_3$ film measured using RSXD diffraction. (b) Plot of the temperature-dependent integrated intensity and (inset) the magnetic modulation vector (q) along the b axis with lowering of temperature derived from the (0 q 0) reflections.

intensity [21,22]. Albeit, azimuthal scans were not conducted on GdMnO$_3$ thin films. Analogous to other o-RMnO$_3$ films (R = Y, Tm, Ho, Lu [21–23]), measuring a finite (0 q 0) intensity strongly suggests that a similar c axis canting of the Mn spins is present. This confirms that the magnetic order is modulated along the b axis with a finite canting of Mn spins toward the c axis both in the ICM and commensurate phase. A similar feature is found in bulk RMnO$_3$ (R = Tm, Lu) [27,35] with a noncollinear order of Mn spins in the E-type phase.

To summarize the magnetic property studies on strained o-RMnO$_3$ (R = Tb–Lu) films using complementary diffraction techniques revealed that the magnetic ground state is an E-type order consistent with electric properties and it is preceded by an ICM phase. The AFM ground state of the highly strained o-GdMnO$_3$ film stays ICM at all temperatures whereas the dielectric measurements strongly suggest that a robust E-type commensurate phase is stabilized.

C. Magneto-electric studies

The measurements of the dielectric response in an external magnetic field is a common experimental approach to study the coupling of the magnetic and electric order parameters in a magnetoelectric multiferroic [2]. A reorientation of the spin structure in a field can induce changes in the dielectric properties and this implies a modification of the microscopic mechanism that drives multiferroicity. For the o-RMnO$_3$ thin films discussed here, the FE polarization points along the a axis ($P \parallel a$) [25]. In Fig. 8, we plot the normalized capacitance $\Delta C = (C(T) - C(50\,\mathrm{K}))/C(50\,\mathrm{K})$, which is proportional to the dielectric constant, along the a axis for both an applied magnetic field $\mu_o H$ along the a ($\mu_o H \parallel P$) and the c axis ($\mu_o H \perp P$).

For the 10-nm thin GdMnO$_3$ film, the normalized capacitance ΔC along the a axis has a cusplike peak and shows a shift of T_{FE} as a function of the magnetic field along the a and the c axis [see Figs. 8(a) and 8(b)]. At zero magnetic field $T_{\mathrm{FE}} \sim 38.3\,\mathrm{K}$ and $\Delta C \sim 3\%$ is close to the results reported previously [25]. The other feature observed is a small humplike increase in ΔC around $T \sim 8\,\mathrm{K}$. This contribution is likely to originate from the induced Gd-ordering below $T_{\mathrm{N}}^{\mathrm{Gd}}$. The application of a magnetic field shifts T_{FE} toward a higher temperature ($\Delta T \sim 0.7\,\mathrm{K}$ at $\mu_o H = 9\,\mathrm{T}$) but the height and shape of ΔC remains unchanged. Also, the small hump at low T is suppressed, implying that the contribution due to Gd-ordering is reduced. These changes in the dielectric properties are independent of the direction of the applied magnetic field. FE ordering occurs at a temperature above the lock-in temperature for E-type ordering ($T_{\mathrm{FE}} > T_{\text{lock-in}}$). This demonstrates the role of the ICM order, which induces FE order. The magnetic-field-dependent change in the dielectric properties thus suggests that the ICM magnetic order is weakly affected by the external magnetic field and causes a small increase in T_{FE}. The magneto-dielectric behavior is, however, independent of the magnetic field direction and suggests the absence of any in-plane anisotropy along the ac plane.

In a 13-nm thin LuMnO$_3$ film, the temperature dependence of ΔC along the a axis showed almost no variation in T_{FE} up to a magnetic field of $\mu_o H = 9\,\mathrm{T}$ [see Figs. 8(c) and 8(d)]. At $T_{\mathrm{FE}} \sim 31\,\mathrm{K}$, $\Delta C \sim 3.5\%$ is unchanged on altering the direction of the applied field. Also, we do not observe any humplike peak at low T, consistent with the absence of a magnetic moment for the R ion. We therefore conclude that the E-type phase, which causes the FE polarization is rigid with respect to an applied magnetic field. This behavior is in agreement with magnetic field dependent electrical property studies of bulk LuMnO$_3$ [3].

D. Multiferroic phase diagram

The present study reveals that the multiferroic properties of strained epitaxial films differ significantly from the variety of magnetic and electric orders observed in bulk o-RMnO$_3$. Bulk RMnO$_3$ experiences a combination of a Jahn Teller distortion and GdFeO$_3$-type rotational distortion of the oxygen octahedron, which both depend on the radius of the R-ion [28,36,37]. This leads to a deviation of the Mn-O-Mn bond angle from the 180° linear configuration. A direct consequence of the inherent structural modification is an R-ion radius dependent variation of the nearest-neighbor (NN) FM and next-nearest-neighbor (NNN) AFM exchange interactions. With decreasing rare-earth ion radius in the RMnO$_3$ series, the magnetic

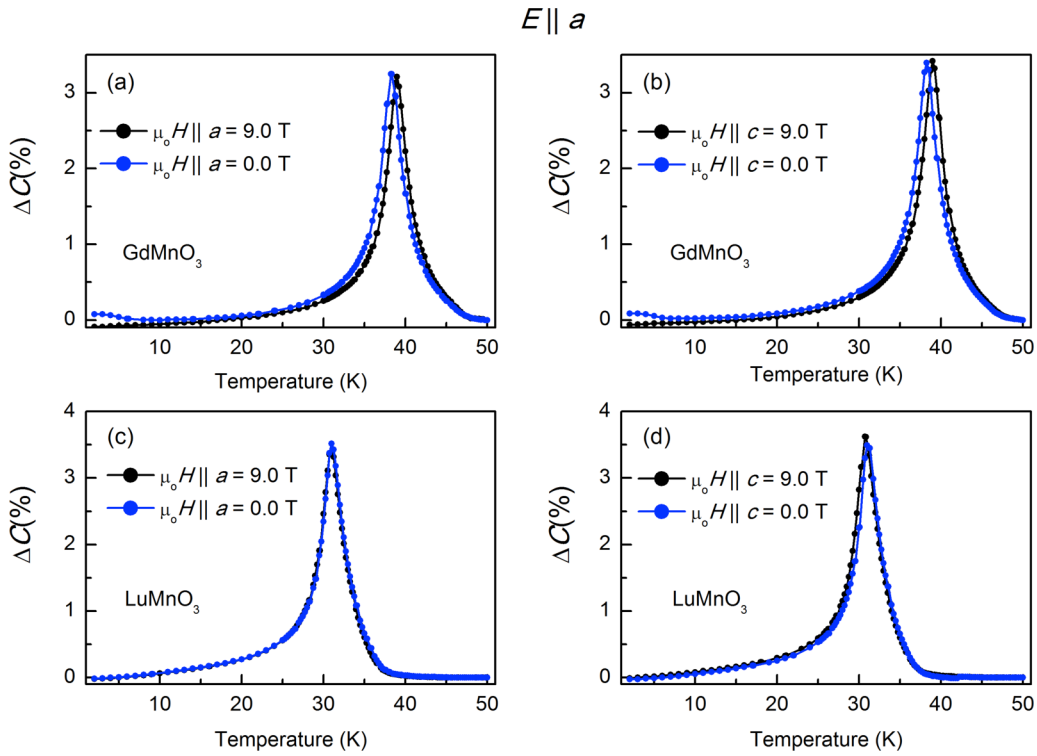

FIG. 8. Normalized capacitance $[\Delta C = (C(T)\text{-}C(50\,\mathrm{K}))/C(50\,\mathrm{K})]$ along the a axis under applied magnetic field ($\mu_o H$) along the a axis ($\mu_o H \parallel P$), and the c axis ($\mu_o H \perp P$) for $GdMnO_3$ in (a) and (b), respectively, and for $LuMnO_3$ in (c) and (d), respectively.

ground state stabilizes into an A-type AFM order for R = Gd. This is followed by a spiral order for R = Tb, Dy [2–4] and an E-type order for R = Ho–Lu, which have the smallest rare-earth radii [26,27,29,38–40]. The spiral order induces a weaker spontaneous FE polarization compared to the E-type order which is related to the microscopic mechanism for multiferroicity. The former is mediated by an antisymmetric inverse Dzyaloshinskii-Moriya interaction, whereas the latter is caused by a symmetric exchange interaction [5,41,42]. For bulk $R\mathrm{MnO_3}$, drastic variations of their multiferroic properties were observed by the application of an external magnetic field or pressure. The most prominent experimental observations are an enhanced FE polarization in $GdMnO_3$ [11] and the stabilization of the E-type order with an increase and switching of the orientation of P for $TbMnO_3$ [8,43]. In both cases, the increase in the FE polarization induced by the E-type order indicates that o-$R\mathrm{MnO_3}$ tend to favour a symmetric exchange striction under the influence of external parameters. Coherently grown $R\mathrm{MnO_3}$ thin films yield similar results, highlighting the unique ability of strain to modify bulk properties in the absence of other external parameters.

Next we will discuss our results with respect to the generic multiferroic phase diagram of o-$R\mathrm{MnO_3}$ as modified by epitaxial strain [25]. In Ref. [25], we presented a generalized multiferroic phase diagram based on strain-induced FE properties in o-$R\mathrm{MnO_3}$. The resulting multiferroic ground state was found to show $P||a$ independent of the R-ion radius and it was assumed that these strain-induced FE properties are consistent with an AFM E-type ground state. Here, we amend this phase diagram by including the observed magnetic phases of these strained films [25] (see Fig. 9). The multiferroic ground state is an E-type AFM for the whole series of coherently strained o-$R\mathrm{MnO_3}$ films investigated, but the onset temperatures of the magnetic phases vary with decreasing rare earth ion radius. A summary of the various magnetic and electric transition temperatures for bulk and film o-$R\mathrm{MnO_3}$ is presented in Table I.

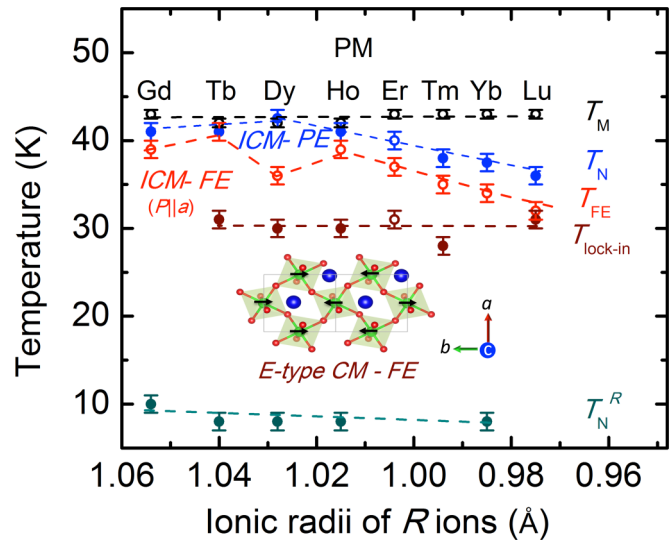

FIG. 9. Multiferroic phase diagram of $R\mathrm{MnO_3}$ showing the R ion radius dependence of magnetic and electric transition temperatures. Values of T_M and T_FE are taken from Ref. [25]. Schematic image of the E-type magnetic order of Mn spins in ab plane shown. The atoms are represented by blue (Lu), green (Mn), and red (O) spheres. Magnitude and direction of spin is drawn as a guide to the eye.

The most prominent features in the phase diagram (Fig. 9) are:

(1) The AFM ordering temperature T_N defined as the onset temperature for magnetic intensity at $(0\,q\,1)$ and $(0\,q\,0)$ shows a variation with the R-ion radius. This is in contrast to the magnetic ordering temperature T_M obtained from magnetic susceptibility measurements on the same set of films, which shows a constant $T_M = 41$ K independent of the R-ion radius [25].

(2) A paralelectric ICM phase exists in the temperature window $T_{FE} < T < T_N$. This phase is also observed in bulk but the temperature range hosting the intermediate ICM phase decreases with decreasing R-ion radius [3,5,37]. For strained films, this behavior is different since an almost congruent ICM-PE region is observed independent of the R-ion radius.

(3) The ICM phase features FE ordering in the temperature window $T_{lock\text{-}in} < T < T_{FE}$ and this region gradually shrinks with decreasing R ionic radius and is absent in $LuMnO_3$.

(4) Below $T_{lock\text{-}in}$, the ground state is described by a commensurate E-type Mn spin order and a large electric polarization along the a axis.

(5) The ordering temperatures for E-type order ($T_{lock\text{-}in}$) do not show any variation. In $GdMnO_3$, the magnetic state approaches the commensurate phase, but does most likely not lock.

(6) The magnetic rare-earth ions order below a temperature T_N^R and induce an abrupt change in the $(0\,q\,1)$ peak intensity for $GdMnO_3$, $HoMnO_3$, and $DyMnO_3$. The overall weak dependence of the ordering temperature on the R ionic radius is consistent with bulk ($T_N^R \sim 4$–7 K) [26,33,34,38] with small variations in the absolute values. Next, we will discuss these features in more detail to give a better insight on the unique modifications of the multiferroic properties.

1. Ordering temperature of the incommensurate phase

In the o-$R\mathrm{MnO_3}$ (R =Gd-Yb) films, an ICM AFM phase appears but the ordering temperature is a puzzling aspect of this multiferroic phase diagram (Fig. 9). There is a clear difference between T_M and T_N when the R-ion radius is smaller than the radius for Ho. All epitaxially strained films show a systematic decrease of T_N with decreasing R-ion radius. As in the bulk, there is an increase in the frustration among the magnetic exchange interactions with decreasing ionic radius leading to a decrease of T_N in these films [34,36]. However, T_M stays invariant with the change in the R radius.

We also note a faint and broad peaklike structure in the magnetic susceptibility at T_M for o-$R\mathrm{MnO_3}$ (R =Er–Lu) and shown for $LuMnO_3$ in Fig. 6(b) (inset) [25]. To explain this feature, we consider the possibility of an additional short range ordering at $T_N < T < T_M$. The zero-field-cooled and field-cooled magnetization curves ($M(T)$) for o-$R\mathrm{MnO_3}$ (R =Er–Lu) have an unusual upward turn or showed small changes at $T < T_M$. Considering the degree of epitaxy [25], we exclude growth-induced defects or residual strain preventing coherent scattering above T_N. Other possible magnetic impurities as a consequence of the deposition process—like inclusions of a very diluted ferrimagnetic Mn_3O_4 phase (∼0.05%) [44,45]—are also ruled out since there is no evidence of an anomaly in the magnetic susceptibility at T_M [25]. Other magnetic impurities as a source for this upward turn, like oxygen trapped in the glue used for the magnetic susceptibility measurements, however, cannot be ruled out since a broad humplike feature in the magnetization curve around $T \sim 43$ K was observed [25,46,47].

2. Electric properties of the incommensurate phase

The electric properties of the ICM phase in the phase diagram depends on the R-ion radius. A paraelectric ICM phase appears, starting with $DyMnO_3$, and exists for films with an R-ion radii smaller than the Dy radius at $T_{FE} < T < T_N$. In the absence of a detailed magnetic structure analysis for the ICM phase, we propose an amplitude modulated spin ordering which retains the crystal symmetry similar to the high temperature ICM paraelectric phase in bulk [3]. The ICM phase shows FE ordering at $T_{FE} \approx T_N$ for R = Gd, Tb with R-ion radii larger than the Dy radius. In addition, and unlike in bulk, T_N and T_{FE} of o-$R\mathrm{MnO_3}$ (R =Dy–Lu) films decrease monotonically with decreasing R radius. Therefore, we propose that an R ion radius larger than 1.027 Å combined with epitaxial strain will favour a significant increase of T_N and T_{FE} in o-$R\mathrm{MnO_3}$.

A similar FE ICM phase in strained o-$R\mathrm{MnO_3}$ films was reported in recent studies without any clear description of the magnetic structure [20,22,23]. Possible candidates proposed include an ab-spiral phase or the coexistence of a CM and an ICM phase, which can induce $P||a$. In addition, the ICM phase vanishes below $T_{lock\text{-}in}$. The significantly larger P in films compared to bulk implies the coexistence of a metastable E-type phase and spiral order above $T_{lock\text{-}in}$, which at low temperatures melt into a homogenous E-type phase [5,23,25]. The other aspect in the phase diagram (Fig. 9) is that the ICM FE phase shrinks with a decreasing R-ion radius, and vanishes for $LuMnO_3$ representing a bulklike behavior [27]. Therefore, in o-$R\mathrm{MnO_3}$ films with R-ion radii smaller than the Dy radius, both the ICM-PE and ICM-FE phase are present, whereas for larger R-ion radii the temperature range for the ICM-PE phase shrinks considerably. These unique strain-induced film properties illustrate the tuning of the microscopic interactions as a function of R ion radius.

3. Origin of the E-type commensurate ferroelectric ground state

An unusual characteristic of the strained films is a robust commensurate E-type ground state independent of the R ion radius, which is consistent with the relatively large electrical polarization [25]. In addition, the lock-in temperature to the E-type phase stays almost constant (Fig. 9). In bulk, a multiferroic E-type phase is found for R = Ho–Lu and theoretically reproduced by Monte Carlo simulations [5,24,25]. They revealed that the relative strength of the NN FM (J_b along the b axis) and the NNN AFM (J_{ab} along the ab axis) exchange interactions play the central role to stabilize an E-type ground state. This can be extended to explain our result and propose a strain-induced variation of the J_b/J_{ab} ratio, which favors the stabilization of the E-type phase [25]. It also implies that strain establishes a symmetric exchange striction as a dominant mechanism to mediate multiferroicity in all these films contrary to bulk [5,48,49].

TABLE II. R ion radii dependence of the lattice parameter ratio.

Rare earth ions	Gd	Tb	Dy	Ho	Er	Tm	Yb	Lu
R (Å) [36]	1.053	1.040	1.027	1.015	1.004	0.994	0.985	0.977
a/b film[25]	0.867	0.872	0.877	0.881	0.886	0.892	0.895	0.897
a/b bulk[28,59,60]	0.906	0.907	0.905	0.901	0.899	0.900	0.899	0.898

In earlier studies, attempts were made to explain the origin of an AFM E-type in strained $R\mathrm{MnO_3}$ films based on the ratio of a and b lattice parameters. These bulk studies showed a systematic decrease in the a/b ratio with decreasing R radius (see Table II). As a result, the multiferroic ground state undergoes transitions from a paraelectric AFM A-type to a FE AFM spin spiral and finally into a FE AFM E-type phase [28,50]. This phenomenological behavior was addressed in $\mathrm{YMnO_3}$ and $\mathrm{DyMnO_3}$ thin films grown on Nb-doped $\mathrm{SrTiO_3}$ showing the dependence of multiferroicity on the a/b parameter [50,51]. The obtained a/b ratios in these films were larger the than bulk values and were proposed to be responsible for the changes in the multiferroic properties. A density-functional theory calculation was performed to explain the stabilization of the E-type order in $\mathrm{TbMnO_3}$ and $\mathrm{HoMnO_3}$ thin films with a compressive ab in-plane strain of $> -4.5\%$ and $< -3\%$, respectively [52,53].

For our o-$R\mathrm{MnO_3}$ thin films, it is not trivial to calculate the ab strain since the a axis experiences a compressive strain whereas the b axis undergoes a change from tensile to compressive strain depending on the R radius [25]. Also, the a/b ratio increases with decreasing R contrary to bulk. However, the a/b ratio of the films (see Table II) always stays lower than the proposed maximum threshold value ($a/b \sim 0.9$) for stabilizing the E-type order. This feature favors the observed E-type phase in our films. A recent systematic first principle study was conducted, which showed that an E-type ground state is favoured in o-$R\mathrm{MnO_3}$ strained thin films for the whole R-ion series if the NN FM interactions gets modified significantly by strain [54]. These studies are in agreement with our results highlighting the role of strain to stabilize a robust multiferroic ground state in o-$R\mathrm{MnO_3}$ films. However, the proposed mechanism in a similar report by Li *et al.* [55] does not represent our results owing to the variation in the strain applied for the (110)-oriented films considered by them.

4. Multiferroic mechanism under magnetic field

The study of the dielectric response in an external magnetic field revealed the sensitivity of the microscopic mechanisms that induces multiferroicity in $\mathrm{GdMnO_3}$ and $\mathrm{LuMnO_3}$ films. The FE order in a $\mathrm{GdMnO_3}$ film (largest R-ion radius) shows a higher sensitivity to the applied magnetic field compared to a $\mathrm{LuMnO_3}$ film (smallest R-ion radius). The existence of an ICM phase showing FE ordering in a strained $\mathrm{GdMnO_3}$ film implies a possible combination of DMI and magnetostriction to be responsible for the FE order. In $\mathrm{LuMnO_3}$ the FE state occurs only in the commensurate phase and points toward the symmetric exchange striction as the dominant mechanism for ferroelectricity. Therefore, our results highlights the rigidity of the symmetric exchange in an applied magnetic field as compared to the antisymmetric exchange interaction.

IV. CONCLUSION

Neutron scattering and x-ray diffraction were used as complementary techniques to identify the magnetic order in coherently grown (010)-oriented o-$R\mathrm{MnO_3}$ (R = Gd–Lu) thin films. We derived a multiferroic phase diagram, which is modified from bulk due to strain effects [3]. The magnetic order of the multiferroic ground state was found to be E-type, consistent with the relatively large spontaneous polarization along the a axis. The FE ordering already occurs in the ICM phase, implying that the commensurate E-type order is not prerequisite for ferroelectricity in the strained films. The magnetic ordering temperature T_N shows an R-ion radius dependent variation, whereas the transition temperature to the E-type order, $T_{\text{lock-in}}$ is almost independent of the R-ion radius. We also present magnetic field dependent FE properties in the ICM phase and identify the interplay of R-ion $4f$ and Mn-ion $3d$ moments. Our study highlights the role of epitaxial strain as an ideal tool to realize high performance multiferroics. We hope that our results will trigger theoretical studies to explain the presented epitaxial strain dependent multiferroic properties in o-$R\mathrm{MnO_3}$ thin films.

ACKNOWLEDGMENTS

Work at the PSI is supported by the Swiss National Foundation (SNF) (Project No. 200021-147049). Financial support and CROSS funding to K.S. from PSI are acknowledged. The work is based on experiments performed at the Swiss Spallation Neutron Source, SINQ and SLS, PSI, Switzerland. A part of the work was also conducted at the ILL, Grenoble, France. Y.W.W. and M.R. acknowledge funding by SNF (Project No. 200021-137657) and CRSII2-147606, respectively. The financial support from the National Center of Competence in Research, Molecular Ultrafast Science and Technology (NCCR MUST), a funding tool of the Swiss National Science Foundation, is acknowledged. The soft x-ray experiments were carried out at X11MA beamline of the SLS, PSI, Villigen, Switzerland. The authors thank the X11MA beamline staff for experimental support. The capacitance measurements under applied magnetic fields were carried out on the PPMS devices of the Laboratory for Developments and Methods, PSI, Villigen, Switzerland.

[1] N. A. Spaldin and M. Fiebig, Science **309**, 391 (2005).

[2] T. Kimura, T. Goto, H. Shintani, K. Ishizaka, T. Arima, and Y. Tokura, Nature **426**, 55 (2003).

[3] S. Ishiwata, Y. Kaneko, Y. Tokunaga, Y. Taguchi, T.-h. Arima, and Y. Tokura, Phys. Rev. B **81**, 100411 (2010).

[4] M. Kenzelmann, A. B. Harris, S. Jonas, C. Broholm, J. Schefer, S. B. Kim, C. L. Zhang, S.-W. Cheong, O. P. Vajk, and J. W. Lynn, Phys. Rev. Lett. **95**, 087206 (2005).

[5] M. Mochizuki, N. Furukawa, and N. Nagaosa, Phys. Rev. B **84**, 144409 (2011).

[6] A. Muñoz, J. A. Alonso, M. T. Casais, M. J. Martínez-Lope, J. L. Martínez, and M. T. Fernández-Díaz, J. Phys.: Condens. Matter **14**, 3285 (2002).

[7] S. Ishiwata, Y. Tokunaga, Y. Taguchi, and Y. Tokura, J. Am. Chem. Soc. **133**, 13818 (2011).

[8] T. Aoyama, K. Yamauchi, A. Iyama, S. Picozzi, K. Shimizu, and T. Kimura, Nat. Commun. **5**, 4927 (2014).

[9] J. M. Chen, T. L. Chou, J. M. Lee, S. A. Chen, T. S. Chan, T. H. Chen, K. T. Lu, W. T. Chuang, H.-S. Sheu, S. W. Chen, C. M. Lin, N. Hiraoka, H. Ishii, K. D. Tsuei, and T. J. Yang, Phys. Rev. B **79**, 165110 (2009).

[10] N. Zhang, S. Dong, Z. Fu, Z. Yan, F. Chang, and J. Liu, Sci. Rep. **4**, 6506 (2014).

[11] T. Aoyama, A. Iyama, K. Shimizu, and T. Kimura, Phys. Rev. B **91**, 081107 (2015).

[12] G. Catalan and J. F. Scott, Adv. Mater. **21**, 2463 (2009).

[13] L. W. Martin, S. P. Crane, Y.-H. Chu, M. B. Holcomb, M. Gajek, M. Huijben, C.-H. Yang, N. Balke, and R. Ramesh, J. Phys.: Condens. Matter **20**, 434220 (2008).

[14] M. Fiebig, T. Lottermoser, D. Meier, and M. Trassin, Nat. Rev. Mater. **1**, 16046 (2016).

[15] J. H. Haeni, P. Irvin, W. Chang, R. Uecker, P. Reiche, Y. L. Li, S. Choudhury, W. Tian, M. E. Hawley, B. Craigo, A. K. Tagantsev, X. Q. Pan, S. K. Streiffer, L. Q. Chen, S. W. Kirchoefer, J. Levy, and D. G. Schlom, Nature **430**, 758 (2004).

[16] J. H. Lee, L. Fang, E. Vlahos, X. Ke, Y. W. Jung, L. F. Kourkoutis, J.-W. Kim, P. J. Ryan, T. Heeg, M. Roeckerath, V. Goian, M. Bernhagen, R. Uecker, P. C. Hammel, K. M. Rabe, S. Kamba, J. Schubert, J. W. Freeland, D. A. Muller, C. J. Fennie, P. Schiffer, V. Gopalan, E. Johnston-Halperin, and D. G. Schlom, Nature **466**, 954 (2010).

[17] D. Rubi, C. de Graaf, C. J. M. Daumont, D. Mannix, R. Broer, and B. Noheda, Phys. Rev. B **79**, 014416 (2009).

[18] X. Martí, V. Skumryev, C. Ferrater, M. García-Cuenca, M. Varela, F. Sánchez, and J. Fontcuberta, Appl. Phys. Lett. **96**, 222505 (2010).

[19] X. Martí, V. Skumryev, V. Laukhin, F. Sánchez, García-Cuenca, C. M. Ferrater, M. Varela, and J. Fontcuberta, J. Mater. Res. **22**, 2096 (2011).

[20] K. Shimamoto, Y. W. Windsor, Y. Hu, M. Ramakrishnan, A. Alberca, E. M. Bothschafter, L. Rettig, T. Lippert, U. Staub, and C. W. Schneider, Appl. Phys. Lett. **108**, 112904 (2016).

[21] Y. W. Windsor, M. Ramakrishnan, L. Rettig, A. Alberca, E. M. Bothschafter, U. Staub, K. Shimamoto, Y. Hu, T. Lippert, and C. W. Schneider, Phys. Rev. B **91**, 235144 (2015).

[22] Y. W. Windsor, S. W. Huang, Y. Hu, L. Rettig, A. Alberca, K. Shimamoto, V. Scagnoli, T. Lippert, C. W. Schneider, and U. Staub, Phys. Rev. Lett. **113**, 167202 (2014).

[23] H. Wadati, J. Okamoto, M. Garganourakis, V. Scagnoli, U. Staub, Y. Yamasaki, H. Nakao, Y. Murakami, M. Mochizuki, M. Nakamura, M. Kawasaki, and Y. Tokura, Phys. Rev. Lett. **108**, 047203 (2012).

[24] K. Shimamoto, S. Mukherjee, S. Manz, J. S. White, M. Trassin, M. Kenzelmann, L. Chapon, T. Lippert, M. Fiebig, C. W. Schneider, and C. Niedermayer, Sci. Rep. **7**, 44753 (2017).

[25] K. Shimamoto, S. Mukherjee, N. S. Bingham, A. K. Suszka, T. Lippert, C. Niedermayer, and C. W. Schneider, Phys. Rev. B **95**, 184105 (2017).

[26] A. Muñoz, M. T. Casáis, J. A. Alonso, M. J. Martínez-Lope, J. L. Martínez, and M. T. Fernández-Díaz, Inorg. Chem. **40**, 1020 (2001).

[27] S. Mukherjee, A. Dönni, T. Nakajima, S. Mitsuda, M. Tachibana, H. Kitazawa, V. Pomjakushin, L. Keller, C. Niedermayer, A. Scaramucci, and M. Kenzelmann, Phys. Rev. B **95**, 104412 (2017).

[28] M. Tachibana, T. Shimoyama, H. Kawaji, T. Atake, and E. Takayama-Muromachi, Phys. Rev. B **75**, 144425 (2007).

[29] F. Ye, B. Lorenz, Q. Huang, Y. Q. Wang, Y. Y. Sun, C. W. Chu, J. A. Fernandez-Baca, P. Dai, and H. A. Mook, Phys. Rev. B **76**, 060402 (2007).

[30] K. Lefmann, C. Niedermayer, A. B. Abrahamsen, C. R. H. Bahl, N. B. Christensen, H. S. Jacobsen, T. L. Larsen, P. Häfliger, U. Filges, and H. M. Rønnow, Physica B: Condensed Matter **385-386**, 1083 (2006).

[31] U. Staub, V. Scagnoli, Y. Bodenthin, M. García-Fernández, R. Wetter, A. M. Mulders, H. Grimmer, and M. Horisberger, J. Synchrotron Radiat. **15**, 469 (2008).

[32] U. Flechsig, F. Nolting, A. Fraile Rodríguez, J. Krempaský, C. Quitmann, T. Schmidt, S. Spielmann, and D. Zimoch, AIP Conf. Proc. **1234**, 319 (2010).

[33] J. Hemberger, S. Lobina, H.-A. Krug von Nidda, N. Tristan, V. Y. Ivanov, A. A. Mukhin, A. M. Balbashov, and A. Loidl, Phys. Rev. B **70**, 024414 (2004).

[34] T. Kimura, G. Lawes, T. Goto, Y. Tokura, and A. P. Ramirez, Phys. Rev. B **71**, 224425 (2005).

[35] M. Garganourakis, Y. Bodenthin, R. A. de Souza, V. Scagnoli, A. Dönni, M. Tachibana, H. Kitazawa, E. Takayama-Muromachi, and U. Staub, Phys. Rev. B. **86**, 054425 (2012).

[36] T. Kimura, S. Ishihara, H. Shintani, T. Arima, K. T. Takahashi, K. Ishizaka, and Y. Tokura, Phys. Rev. B **68**, 060403 (2003).

[37] T. Goto, T. Kimura, G. Lawes, A. P. Ramirez, and Y. Tokura, Phys. Rev. Lett. **92**, 257201 (2004).

[38] Y. H. Huang, H. Fjellvåg, M. Karppinen, B. C. Hauback, H. Yamauchi, and J. B. Goodenough, Chem. Mater. **18**, 2130 (2006).

[39] V. Y. Pomjakushin, M. Kenzelmann, A. Dönni, A. B. Harris, T. Nakajima, S. Mitsuda, M. Tachibana, L. Keller, J. Mesot, H. Kitazawa, and E. Takayama-Muromachi, New J. Phys. **11**, 043019 (2009).

[40] H. Okamoto, N. Imamura, B. Hauback, M. Karppinen, H. Yamauchi, and H. Fjellvåg, Solid State Commun. **146**, 152 (2008).

[41] M. Mochizuki and N. Furukawa, Phys. Rev. B **80**, 134416 (2009).

[42] M. Mochizuki, Phys. Rev. B **92**, 224412 (2015).

[43] N. Terada, D. D. Khalyavin, P. Manuel, T. Osakabe, A. Kikkawa, and H. Kitazawa, Phys. Rev. B **93**, 081104 (2016).

[44] R. Nath, K. M. Ranjith, B. Roy, D. C. Johnston, Y. Furukawa, and A. A. Tsirlin, Phys. Rev. B **90**, 024431 (2014).

[45] D. G. Tomuta, S. Ramakrishnan, G. J. Nieuwenhuys, and J. A. Mydosh, J. Phys.: Condens. Matter **13**, 4543 (2001).

[46] Phase transition in magnetic susceptibility due to trapped oxygen contamination is addressed by Quantum Design in their manual for MPMS under application note 1014-210.

[47] S. Gregory, Phys. Rev. Lett. **40**, 723 (1978).

[48] I. A. Sergienko, C. Şen, and E. Dagotto, Phys. Rev. Lett. **97**, 227204 (2006).
[49] B. Lorenz, Y. Q. Wang, Y. Y. Sun, and C. W. Chu, Phys. Rev. B **70**, 212412 (2004).
[50] J. Fontcuberta, I. Fina, L. Fàbrega, F. Sánchez, X. Martí, and V. Skumryev, Phase Transitions **84**, 555 (2011).
[51] C. Lu, S. Dong, Z. Xia, H. Luo, Z. Yan, H. Wang, Z. Tian, S. Yuan, T. Wu, and J. Liu, Sci. Rep. **3**, 3374 (2013).
[52] Y. S. Hou, J. H. Yang, X. G. Gong, and H. J. Xiang, Phys. Rev. B **88**, 060406 (2013).
[53] D. Iuşan, K. Yamauchi, P. Barone, B. Sanyal, O. Eriksson, G. Profeta, and S. Picozzi, Phys. Rev. B **87**, 014403 (2013).
[54] J. T. Zhang, C. Ji, J. L. Wang, W. S. Xia, X. M. Lu, and J. S. Zhu, Phys. Rev. B **97**, 085124 (2018).
[55] G. Li, X. Huang, J. Hu, G. Song, and W. Zhang, Phys. Rev. B **97**, 085140 (2018).
[56] T. Arima, T. Goto, Y. Yamasaki, S. Miyasaka, K. Ishii, M. Tsubota, T. Inami, Y. Murakami, and Y. Tokura, Phys. Rev. B **72**, 100102 (2005).
[57] H. Kuwahara, K. Noda, J. Nagayama, and S. Nakamura, Physica B: Condensed Matter **359-361**, 1279 (2005).
[58] O. Prokhnenko, R. Feyerherm, M. Mostovoy, N. Aliouane, E. Dudzik, A. U. B. Wolter, A. Maljuk, and D. N. Argyriou, Phys. Rev. Lett. **99**, 177206 (2007).
[59] T. Mori, N. Kamegashira, K. Aoki, T. Shishido, and T. Fukuda, Mater. Lett. **54**, 238 (2002).
[60] J. A. Alonso, M. J. Martínez-Lope, M. T. Casais, and M. T. Fernández-Díaz, Inorg. Chem. **39**, 917 (2000).